Pis'ma v ZhETF, vol. 82, iss. 9, pp. 678 – 681

Surface-plasmon vortices in nanostructured metallic films

A. A. Ezhov[1)], *S. A. Magnitskii, N. S. Maslova, D. A. Muzychenko, A. A. Nikulin, V. I. Panov*

Department of Physics, M. V. Lomonosov Moscow State University, 119992 Moscow, Russia

Submitted 29 August 2005

Resubmitted 27 September 2005

Light scattering by a small protrusion on a metal surface is analyzed within the framework of perturbation theory. Upon normal incidence of linearly-polarized monochromatic wave, slight deviations of the protrusion shape from a circularly symmetric one lead to formation of optical vortices in the near-field region due resonant excitation of circular surface plasmons. This agrees with the results of scanning near-field optical microscopy experiments revealing distinct spiral patterns in the in-plane near-field intensity distribution for metallized nanostructured polymer substrates.

PACS: 74.50.+r, 74.80.Fp

In the past decade, phase singularities of optical wave fields have attracted considerable interest in both fundamental and applied aspects. There are numerous techniques to produce an optical field with a screw dislocation (optical vortex) [1, 2]. Optical vortices produced by phase steps – refracting or reflecting surface structures shaped into one turn of a helicoid – can be understood in terms of the Berry phase and, in essential respects, have analogy with Aaronov-Bohm effect. Phase singularities can play a significant role in interaction of light with solid state structures being developed for modern nanophotonic applications.

Introducing scanning near-field optical microscopy (SNOM) [3] as an experimental method has allowed investigating phase singularities with the sub-wavelength resolution. Phase singularities of optical fields in waveguide structures [4] and in the focal region of a lens [5] have been observed by means of interferometric SNOM.

Recently, distinct spiral patterns in the in-plane near-field fringes [6] have been detected by SNOM measurements of the three-dimensional distribution of the field intensity near nanocylinders irradiated by linearly-polarized monochromatic light incident normally to the axes of the nanocylinders. Constant wave laser beam with wavelength 532 nm was additionally polarized by the Nicole prism with the extinction ratio $5 \cdot 10^{-5}$ at the most. The nanocylinders were manufactured by double replication from a silicon matrix and placed onto a polymer substrate. Some of the nanocylinders were covered by gold-palladium 20–30 nm-thick layer, the coverage non-uniformity due to the shadow effect being prevented by the coating procedure. According to Fig.1, the unexpected interference patterns with a spiral symmetry were observed only for metallized samples, whereas for bare (not metallized) ones the patterns were circular.

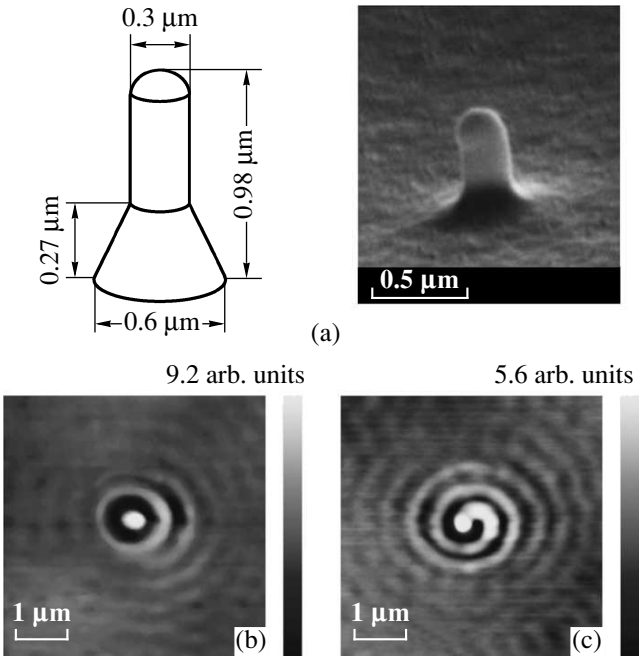

Fig.1. Geometric parameters and scanning electronic microscope image of a polymer nanocylinder (a); SNOM image of the near-field intensity distribution near a bare polymer nanocylinder (b) and that coated by a 25 nm-thick gold-palladium layer (c) measured at the height of 20 nm above the cylinder tops upon normal incidence of linearly-polarized light with wavelength of 532 nm

These experimental results can be understood on a qualitative level by considering a model that admits the use of a simplified perturbation-theory procedure as compared to those developed in the context of a more general approach [7, 8]. A linearly-polarized plane wave

[1)] e-mail: spm@spmlab.phys.msu.su

with frequency ω is incident from vacuum at a normal to the boundary of a semi-infinite metal occupying the half-space $z < Z(\rho, \varphi)$, where ρ, φ, z are the cylindrical coordinates and the function $Z(\rho, \varphi)$ describes a nearly flat surface having a single protrusion with height L and radius R:

$$Z(\rho, \varphi) = L f(\rho/R)\,[1 + \gamma\, g(\varphi)]\,, \tag{1}$$

where the function $f(x)$ satisfies the conditions

$$f(x < 1) > 0,\ f(x \geq 1) \equiv 0 \tag{2}$$

and the term $\gamma\, g(\varphi)$ describes deviations of the protrusion shape from a circularly symmetric one. Taking these circular-symmetry shape distortions into account is of primary importance for the model, since another factor breaking the symmetry between clockwise and counterclockwise directions – the presence of a circularly-polarized component in the incident radiation – is excluded by the experimental procedure. The surface defect is assumed to be (i) slightly sloping, (ii) small in comparison to the wave penetration depth in the metal, and (iii) having small circular-symmetry distortions, i.e.

$$L \ll R \ll \frac{c}{\omega\sqrt{|\varepsilon|}},\ \gamma \ll 1 \tag{3}$$

with ε being the dielectric constant of the metal. We suppose that $-\mathrm{Re}\,\varepsilon(\omega) \gg 1$ and simplify the boundary-value problem of finding the scattered electromagnetic field outside the metal by the use of the impedance boundary conditions at $z = Z(\rho, \varphi)$:

$$\mathbf{E}_t = \zeta\,[\mathbf{H}_t\ \mathbf{n}]\,, \tag{4}$$

where $\mathbf{E}$ and $\mathbf{H}$ are the electric and magnetic fields at frequency ω, respectively, $\zeta = \sqrt{1/\varepsilon}$ is the surface impedance of the metal, $\mathbf{n}$ is the unit vector normal to the surface and directed inward the metal, the subscript t denotes the value of the tangential vector component taken at $z = Z(\rho, \varphi)$. In case of a perfectly flat boundary $z = 0$ the approximate boundary conditions (4) yield the following relation between the wave number q and frequency Ω of a surface plasmon wave propagating along the plane $z = 0$ (the inverse function determines the dispersion law):

$$q = \frac{\Omega}{c}\sqrt{1 + \zeta(\Omega)^2},\quad |\zeta| \ll 1. \tag{5}$$

This result reproduces the exact relation $q = \Omega/c\sqrt{1 - \zeta(\Omega)^2}$ to the second order in ζ inclusive.

It is convenient to represent the total field $\mathbf{F}$ at $z \geq Z(\rho, \varphi)$ as a sum of four terms (here $\mathbf{F}$ stands for either $\mathbf{E}$ or $\mathbf{H}$)

$$\mathbf{F} = \mathbf{F}_0\, e^{-ikz} + \bar{\mathbf{F}}\, e^{ikz} + \mathbf{F}^{(\mathrm{s})}(\rho, \varphi)\, e^{-\kappa_\mathrm{s} z} + \tilde{\mathbf{F}}(\rho, \varphi, z), \tag{6}$$

where $\kappa_\mathrm{s} = \sqrt{q_\mathrm{s}^2 - k^2}$, $k = \omega/c$, q_s is the wavevector modulus of the surface-plasmon wave at frequency ω (i.e. q_s the root of the equation $\Omega\,(q_\mathrm{s}) = \omega$ with $\Omega(q)$ being the function inverse to that given by Eq. (5)). The vector $\mathbf{F}_0$ is the field amplitude in the incident wave, $\bar{\mathbf{E}} = (\zeta - 1)/(1 + \zeta)\ \mathbf{E}_0$, $\bar{\mathbf{H}} = -(\zeta - 1)/(1 + \zeta)\ \mathbf{H}_0$, $\mathbf{F}^{(\mathrm{s})}$ and $\tilde{\mathbf{F}}$ are the functions to be found. The first two terms in Eq. (6) correspond to a superposition of the incident wave and that reflected from the flat boundary $z = 0$. The third term in Eq. (6) stems from resonant excitation of surface plasmons. The far-field contribution to the field scattered by the protrusion is included in the remainder term $\tilde{\mathbf{F}}$.

We assume that at the boundary the field $\tilde{\mathbf{F}}$ is negligible against the background of the surface-plasmon term in the following sense:

$$\left|\tilde{\mathbf{F}}\right|_{z=Z(\rho,\varphi)} \ll \left|\mathbf{F}^{(\mathrm{s})}\right|,\quad \left|\frac{\partial\tilde{\mathbf{F}}}{\partial z}\right|_{z=Z(\rho,\varphi)} \ll \kappa_\mathrm{s}\left|\mathbf{F}^{(\mathrm{s})}\right|. \tag{7}$$

It will be shown that the procedure of finding $\mathbf{F}^{(\mathrm{s})}$ based on conditions (7) is self-consistent, i.e. it guarantees their fulfilment. The field $\mathbf{F}^{(\mathrm{s})}(\rho, \varphi)$ can be expanded in the Fourier series

$$\mathbf{F}^{(\mathrm{s})}(\rho, \varphi) = \sum_n \mathbf{F}_n(\rho) e^{in\varphi}. \tag{8}$$

The four of six vector components of $\mathbf{E}_n(\rho)$ and $\mathbf{H}_n(\rho)$ can be explicitly expressed from the Maxwell equations through the remaining two, $E_{z,n}(\rho) \equiv E_n(\rho)$ and $H_{z,n}(\rho) \equiv H_n(\rho)$.

At $\rho > R$ the functions $E_n(\rho)$ and $H_n(\rho)$ correspond to the normal field components in a travelling (diverging) circular surface-plasmon wave with the wave number q_s. Hence,

$$E_n(\rho > R) = C_n H^{(1)}_{|n|}(q_\mathrm{s}\rho), \tag{9}$$

$$H_n(\rho > R) \equiv 0, \tag{10}$$

where $H^{(1)}_{|n|}(x)$ is the Hankel function of first kind and C_n is a constant. Thus the problem reduces to finding the functions $E_n(\rho)$ and $H_n(\rho)$ within the interval $0 \leq \rho \leq R$. At $\rho = R$ they should be sewed

together with the functions given by Eq. (9) to provide continuity of all field components. The function $g(\varphi)$ in Eq. (1) can be expanded in the Fourier series: $g(\varphi) = \sum_{n\neq 0} g_n e^{in\varphi}$ with $g_{-n} = g_n^*$. We approximate the exponential factors in Eq. (6) at $z = Z(\rho,\varphi)$ by two lowest-order terms in their Taylor-series expansions at $z = 0$: $e^{\pm ikZ(\rho,\varphi)} \approx 1 \pm ikZ(\rho,\varphi)$ and limit ourselves to the first order in the small parameter kL. In this way the boundary conditions (4) are mapped onto the plane $z = 0$. Within the chosen accuracy we obtain that $E_{n\neq\pm1} = H_{n\neq\pm1} \equiv 0$, meanwhile $E_{n=\pm1}$ and $H_{n=\pm1}$ satisfy the following set of equations (where the prime denotes the first derivative of a function and $\xi \equiv \rho/R$):

$$n\left[-H_n(\xi) + 2\gamma_n\alpha(\xi)H_{-n}(\xi)\right] + \\ + \xi\alpha'(\xi)\left[E_n(\xi) + \gamma_n E_{-n}(\xi)\right] = is(\xi), \qquad (11)$$

$$i\xi H_n'(\xi) + \xi\alpha'(\xi)\left[H_n(\xi) + \gamma_n H_{-n}(\xi)\right] - \\ - 2n\gamma_n\alpha(\xi)E_{-n} = -ns(\xi), \qquad (12)$$

$$n = \pm 1\,,\ 0 \le \xi \le 1\,,$$

with $\gamma_1 = \gamma_{-1}^* = \gamma g_2$, $\alpha(\xi) = kLf(\xi)$, and $s(\xi) = k^2RL(1-\zeta)E_0\xi f(\xi)$. The main feature of this equation set is breaking of symmetry between the terms with $n = 1$ and those with $n = -1$. The analysis of the relative magnitude of the coefficients in Eqs. (11), (12) shows that $|E_n(\rho < R)| \gg |H_n(\rho < R)|$. Taking this into account, we neglect $H_n(\rho < R)$ to provide continuity of the field components at $\rho = R$. At $\xi \to 0$ it follows from Eqs. (11), (12) that $E_n(\xi) \propto \xi$. At $\xi \approx 1$ and $f(\xi) = 1 - \xi$ Eqs. (11), (12) yield the following approximate expressions for $E_{\pm1}$:

$$E_{\pm1}(\eta) \approx A_{\pm1}e^{\gamma|g_2|\eta^2/2} + B_{\pm1}e^{-\gamma|g_2|\eta^2/2} + \\ + kR(1-\zeta)\left(i\eta + 2\gamma_{\pm1}\eta^3\right), \qquad (13)$$

where $\eta \equiv 1-\xi \ll 1$ and the constants $A_{\pm1}$ and $B_{\pm1}$ are to be found simultaneously with $C_{\pm1}$ entering into Eq. (9). We extrapolate the expressions given by Eq. (13) to the whole interval $0 \le \xi \le 1$ with the extra boundary condition $E_{\pm1}(\xi = 0) = 0$. The latter, together with the sewing conditions at $\xi = 1$ provides equations for determining the constants $A_{\pm1}$, $B_{\pm1}$ and $C_{\pm1}$. As a result, we obtain

$$A_{\pm1} = \frac{1}{2}\left(\frac{q_s Rh'}{\gamma|g_2|} + h\right)C_{\pm1}, \qquad (14)$$

$$B_{\pm1} = \frac{1}{2}\left(-\frac{q_s Rh'}{\gamma|g_2|} + h\right)C_{\pm1}, \qquad (15)$$

$$C_{\pm1} = \frac{kR(\zeta-1)\left(\frac{3}{2}\gamma_{\pm1} + i\right)E_0}{q_s Rh'\sinh\frac{\gamma|g_2|}{2} + h\cosh\frac{\gamma|g_2|}{2}}, \qquad (16)$$

where

$$h = H_1^{(1)}(q_s R), \quad h' = \frac{1}{2}\left(H_0^{(1)}(q_s R) - H_2^{(1)}(q_s R)\right).$$

Finally, we should check that the found solutions are consistent with the initial assumptions given by inequalities (7). Since the sum $E_z^{(s)}(\rho,\varphi)\,e^{-\kappa_s z} + \tilde{E}_z(\rho,\varphi,z)$ from Eq. (6) satisfies the three-dimensional Helmholtz equation with the wavevector modulus ω/c, the function $\tilde{E}_z(\rho,\varphi,z)$, within the chosen accuracy, has the integral form

$$\tilde{E}_z(\mathbf{r}) = \int\limits_{\substack{\rho'<R \\ z'>Z(\rho,\varphi)}} G(|\mathbf{r}-\mathbf{r}'|)\,(\Delta_{\rho',\varphi'} + q_s^2)E_z^{(s)}(\mathbf{r}')\,d^3r', \qquad (17)$$

where

$$G(r) = \frac{\exp(ikr)}{4\pi r}, \quad \Delta_{\rho,\varphi} = \frac{1}{\rho}\frac{\partial}{\partial\rho}\left(\rho\frac{\partial}{\partial\rho}\right) + \frac{1}{\rho^2}\frac{\partial^2}{\partial\varphi^2}$$

and $E_z^{(s)}(\mathbf{r}) = E_z^{(s)}(\rho,\varphi)\,e^{-\kappa_s z}$. From Eq. (17) the following estimations can be obtained

$$\left|\frac{\tilde{E}_z\Big|_{z=Z(\rho,\varphi)}}{E_z^{(s)}}\right| \sim (kR)^2 \ll 1, \qquad (18)$$

$$\left|\frac{\dfrac{\partial\tilde{E}_z}{\partial z}\Big|_{z=Z(\rho,\varphi)}}{\kappa_s E_z^{(s)}}\right| \sim \sqrt{|\varepsilon|}\,(kR)^2 \ll 1, \qquad (19)$$

which leads to inequalities (7).

Analyzing the spatial behavior of the non-vanishing time-averaged characteristics of the scattered field, we conclude that for the found solution a first-order vortex occurs in the in-plane distribution of the tangential component of the time-averaged Poynting vector $\mathbf{S} = \frac{c}{8\pi}\mathrm{Re}\,[\mathbf{E}\,\mathbf{H}^*]$ taken at the metal boundary $z = Z(\rho,\varphi)$. The projection of $\mathbf{S}$ onto the plane $z = 0$ describes the energy flow in the travelling surface-plasmon wave resonantly excited by the incident light due to the presence of the surface defect. This component exponentially decays as $|z|$ grows and it is lacking in the absence of the surface plasmon, e.g., at a dielectric substrate with $\mathrm{Re}\,\varepsilon > 0$. For our model we obtain:

$$\left|S_x^{(s)}\right| \gg \left|S_y^{(s)}\right|, \qquad (20)$$

$$S_x^{(s)} = \frac{c\,e^{-\kappa_s z}}{4\pi}\mathrm{Re}\left(E_z^{(s)}(\rho,\varphi)\,E_0^*\right) \propto$$
$$\propto e^{-\kappa_s z}\mathrm{Re}\left\{H_1^{(1)}(q_{sR})(\sin\varphi + \gamma\,\mathrm{Im}\,g_2\,e^{i\varphi})\right\}, \qquad (21)$$

where the x-axis is chosen to be parallel to the electric field $\mathbf{E}_0$ in the incident plane wave. Figure 2 shows the first-order vortex occurring in the in-plane spatial dependence of $S_x^{(s)}(\rho,\varphi,z=Z(\rho,\varphi))$ at $\gamma \neq 0$, i.e. when the defect shape deviates from a circularly symmetric one.

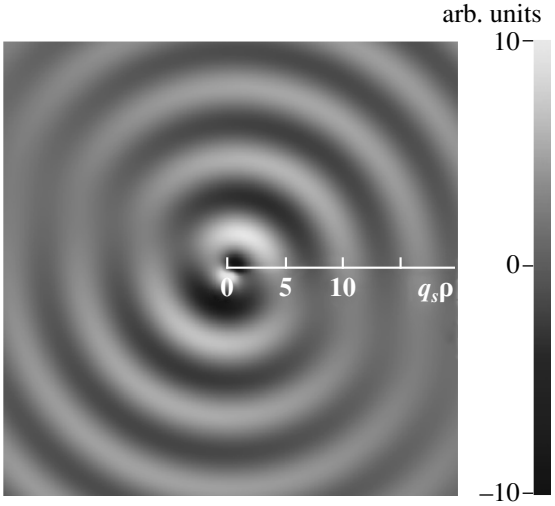

Fig.2. Density plot of the tangential Poynting vector component $S_x^{(s)}$ at the metal surface as a function of the dimensionless radius $q_s\rho$ and polar angle φ ($\gamma = 0.5$, $g_2 = i$)

To summarize, the scattering of linearly polarized monochromatic light by an individual sub-wavelength protrusion in thin metal film has been studied within the framework of perturbation theory. It is shown that even at normal incidence small deviations from circular symmetry of the protrusion shape can result in optical vortex formation in the near-field region if resonant circular surface-plasmon waves are excited. This coincides with the fact that the in-plane near-field intensity distribution measured by scanning near-field optical microscopy has distinct spiral patterns for metallized nanostructured polymer substrates contrary to circular patterns observed for unmetallized substrates where surface-plasmon waves are lacking.

The work was partially supported by RFBR Grants # 03-02-16807, # 04-02-16847, # 04-02-17059. Support from the Samsung Corporation is also gratefully acknowledged.

1. M. V. Berry and J. F. Nye, Proc. Royal Soc. (London) **35**, 8723 (1987).
2. E. Engel, N. Huse, T. A. Klar, and S. W. Hell, Appl. Phys. B **77**, 11 (2003).
3. D. W. Pohl, W. Denk, and M. Lanz, Appl. Phys. Lett. **44**, 651 (1984).
4. M. L. M. Balistreri, J. P. Korterik, L. Kuipers, and N. F. van Hulst, Phys. Rev. Lett. **85**, 294 (2000).
5. J. N. Walford, K. A. Nugent, A. Roberts, and R. E. Scholten, Opt. Lett. **27** 345 (2002).
6. M. V. Bashevoy, A. A. Ezhov, S. A. Magnitskii et al., Int. J. Nanoscience **3**, 105 (2004).
7. P. I. Arseyev, Pis'ma v ZhETF **45**, 132 (1987).
8. P. I. Arseyev, ZhETF **92**, 464 (1987).